

Cross-Scale Pretraining: Enhancing Self-Supervised Learning for Low-Resolution Satellite Imagery for Semantic Segmentation

John Waithaka[✉]

Carnegie Mellon University Africa
Kigali, Rwanda
jwaithak@andrew.cmu.edu

Gustave Bwirayesu[✉]

Carnegie Mellon University Africa
Kigali, Rwanda
gbwiraye@andrew.cmu.edu

Moise Busogi[✉]

Carnegie Mellon University Africa
Kigali, Rwanda
mbusogi@andrew.cmu.edu

Abstract—Self-supervised pretraining in remote sensing is mostly done using mid-spatial resolution (MR) image datasets due to their high availability. Given the release of high-resolution (HR) datasets, we ask how HR datasets can be included in self-supervised pretraining to enhance MR image representation learning and downstream segmentation performance on MR tasks. We design a spatial affinity component that can be added to existing self-supervised learning frameworks and that uses HR imagery to learn better representations of MR imagery. We test the spatial affinity component on two self-supervised learning frameworks and show that it outperforms models pretrained on HR or MR images alone.

Index Terms—remote sensing, satellite imagery, self-supervised learning, super-resolution, semantic segmentation.

I. INTRODUCTION

Semantic segmentation is an important task in remote sensing, enabling, for example, the extraction of crop cover, forest cover, flood extent and marine pollution maps from satellite imagery for applications in food security, disaster management, environmental monitoring, and climate research. While deep learning has excelled in this task, its performance is limited by the scarcity of pixel-level annotations in Earth Observation, which are costly to acquire. Pretraining is commonly used to improve task performance in such annotation-scarce settings. In particular, Self-Supervised Learning (SSL) is a fitting approach for the remote sensing field, where annotations are scarce but imagery data are abundant [1, 2].

Unlike general computer vision, remote sensing has multi-sensor multi-spatial resolution imagery data (aligned by geolocation). Higher resolution (HR) datasets naturally yield superior performance on tasks like semantic segmentation and object detection due to their richer spatial detail [3]. However, HR imagery is often costly, proprietary, or subject to access restrictions. Conversely, mid-resolution (MR) datasets are much more accessible but yield suboptimal task performance. Most remote sensing SSL literature has focused on MR imagery (i.e. $\geq 10\text{m}$ ground sample distance (GSD)) datasets such as Sentinel 1 and Sentinel 2 for pretraining [2, 4–9]. We argue that this is because of the high availability of massive and diverse MR datasets suitable for self-supervised pretraining, rather than any inherent performance advantage.

Recently, large and diverse high-resolution (i.e. $\leq 5\text{m}$ GSD) and mid-resolution image pair datasets such as Sen2Venus [10] have been made public, allowing pretraining with HR data. A straightforward approach would be to pretrain on the HR data alone as in DINOv3 [11]. However, in following this approach, we lose the benefits of mid-resolution satellite imagery such as the higher spectral dimension of most mid-resolution satellite imagery, which has been shown to improve transfer performance [2]. Further, most downstream tasks will use mid-resolution imagery for input due to its high availability. Intuitively, a pretrained model that has not encountered mid-resolution imagery during pretraining may not transfer as well on mid-resolution downstream datasets as one that has.

Therefore, in order to exploit the richer visual detail of HR satellite images without losing the benefits of MR images, we propose a cross-scale pretraining strategy using a real high- and mid-resolution pair dataset; specifically, we use the high-resolution images to learn richer representations of the mid-resolution images. To achieve this, we design the simple *spatial affinity component* that can be added to existing SSL schemes. This component’s purpose is to learn mid-resolution image patch representations that contain the level of spatial detail present in high-resolution images.

We compare models pretrained solely with HR or MR satellite imagery and one pretrained with both HR and MR imagery with the spatial affinity component. We find that adding the spatial affinity component and training with real HR and MR image pair data outperforms pretraining solely with HR or MR imagery.

II. RELATED WORK

A. Self-Supervised Learning for Remote Sensing

Self-supervised learning for remote sensing has gained significant attention in recent years. Since there are massive remote sensing imagery datasets, only very few of which are annotated, SSL naturally fits the remote sensing domain. SSL is used to pretrain foundation models, which are then tuned for specific downstream applications. Most earlier works in SSL for remote sensing use contrastive learning strategies [12–15], which learn by maximising similarity between the embeddings

of related samples and minimising similarity of unrelated samples. Recently, however, focus has shifted to masked image modelling (MIM) [16, 2, 4, 17, 5, 7, 6]. MIM strategies learn by reconstructing masked pixels or patch representations [18, 19]. The state-of-the-art remote sensing SSL frameworks are MIM models.

Most of the existing SSL frameworks are pretrained with MR satellite image datasets. We argue that this is because mid-resolution datasets (e.g. Sentinel 1/2) are much more available than higher resolution datasets, and not because this is optimal. We compare the downstream performance of models pretrained with HR data only, MR data only, and both HR and MR data.

B. Multi-resolution SSL for Remote Sensing

Among the various SSL algorithms for remote sensing, some include a component of super-resolution to enable generalisation across multiple resolutions of satellite imagery. These are Scale-MAE [4] and Cross-Scale MAE [17]. These schemes mathematically downsample high-resolution imagery [20] to get the lower resolution counterpart, which is then included in solving the schemes' pretext tasks. However, research on super-resolution [21, 22] show that downsampling high-resolution images to get a low-resolution counterpart is much less effective than using a real low-resolution counterpart since downsampling cannot reproduce the physical and sensor-specific characteristics of a real low-resolution image. We pretrain on datasets with real low- and high-resolution pairs.

C. Latent-Space Super-Resolution

Much of the research in super-resolution focus on super-resolution in pixel-space. Often, the end goal of these works is a higher resolution image. Our work is inspired by Perception-GAN (PGAN) [23] which does the super-resolution in latent-space. This involves getting the latent representations for both high- and low-resolution images then minimizing the error between them. PGAN and other works that do super-resolution in latent-space primarily use super-resolution as a means of improving performance on another end goal, such as vehicle detection in satellite imagery [24] and general small object detection [23]. Our spatial affinity component can be viewed as a latent-space super-resolution component - a means of learning to represent low-resolution satellite images with the level of spatial and visual detail only contained in higher resolution satellite images.

D. LatentMIM and I-JEPA

To test whether our spatial affinity component generalises across different SSL algorithms, we evaluate it on two SSL schemes - LatentMIM [19] and I-JEPA [25]. Both are masked image modelling schemes that reconstruct patch representations rather than pixels. They use a sampled set of image patches (visible patches) to predict the latent representations of the other patches (masked patches). I-JEPA samples the masked patches as blocks and the visible patches block thus becomes the complement of these (See Fig. 2 (a)). LatentMIM

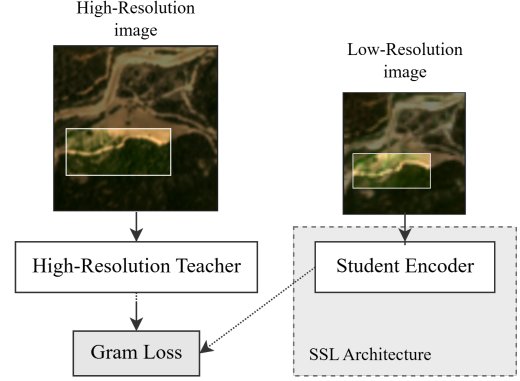


Fig. 1. **Spatial affinity component** samples patches from the high- and mid-resolution inputs. It uses the SSL framework's encoder to encode the lower resolution image and an added high-resolution teacher to encode the high-resolution input. The resulting representations from either encoder are used to compute the gram loss.

samples a random set of non-contiguous patches, $\sim 10\%$ of an image's patches, and the rest become the masked patches. The decoder, which is responsible for the reconstruction, takes the visible patch representations and *mask tokens* as input in both settings. Mask tokens are placeholders for the masked patch representations. The I-JEPA decoder passes the two sets of inputs through several self-attention layers and outputs the processed mask tokens as the predicted mask patch representations. The LatentMIM decoder, on the other hand, passes the two sets of inputs through cross-attention layers such that the mask tokens are processed conditioned on the visible patch representations.

III. METHODOLOGY

A. Spatial Affinity Component

In order to learn mid-resolution image patch representations with the level of spatial detail approaching that of counterpart high-resolution images, we design a spatial affinity component. The spatial affinity component is designed to be added to existing SSL frameworks (see Fig. 1). It has a student-teacher architecture for self-distillation [26]. The student encoder takes patches of the mid-resolution image as input and is updated through backpropagation during training. The student encoder is shared by the SSL scheme and the spatial affinity component. The teacher encoder takes patches of the high-resolution image as input, and we thus call it the *high-resolution teacher*. This high-resolution teacher has the same architecture as the student encoder and its parameters are updated through an exponential moving average of the student encoder's parameters to prevent collapse [26].

a) Inputs: To maintain the image size difference between the mid-resolution image I_{MR} (of size $H_{\text{MR}} \times W_{\text{MR}}$) and its high-resolution counterpart I_{HR} (of size $H_{\text{HR}} \times W_{\text{HR}}$), we use a scale factor of s such that

$$\frac{H_{\text{HR}}}{H_{\text{MR}}} = \frac{W_{\text{HR}}}{W_{\text{MR}}} = s \quad (1)$$

We use $s = 2$.

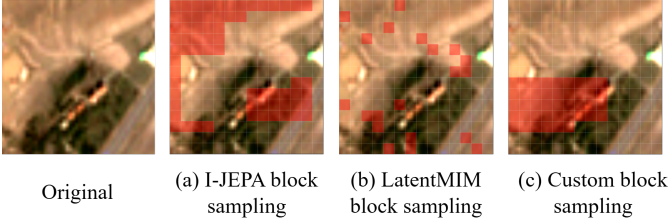


Fig. 2. Patch sampling strategies used by the spatial affinity component and SSL frameworks

As with standard Vision Transformers (ViTs) [27], both images are divided into non-overlapping $P \times P$ patches. The input to the student encoder is a set of patches sampled from the mid-resolution image, I_{MR} . We use the default sampling strategies that the host SSL frameworks use (see Fig. 2 (a) and (b) for I-JEPA and LatentMIM resp.) We also perform ablations on custom block sampling (see Fig. 2 (c)).

Due to the size difference between the image pairs, each patch in I_{MR} corresponds to s^2 patches in I_{HR} . If (u, v) is the 2D coordinate of a patch in I_{MR} , the corresponding set of patches in I_{HR} would have coordinates $\{(s \cdot u + i, s \cdot v + j) \mid 0 \leq i, j < s\}$. After encoding, the set of s^2 patch representations corresponding to a patch in I_{MR} is downsampled to one representation, to match the size of the student encoder output. We perform ablations on bilinear, bicubic and linear projection downsampling methods.

b) Gram loss: We use gram loss as introduced in DINOv3 [11]. This is the mean squared error of the gram matrices of the student encoder output and the downsampled high-resolution teacher output. The gram matrix is a pairwise dot product of \mathbf{L}_2 -normalised patch representations. Let $Z_S \in \mathbb{R}^{N \times d}$ (respectively $Z_T \in \mathbb{R}^{N \times d}$) be the \mathbf{L}_2 -normalised patch representations of the student encoder (respectively the high-resolution teacher, after downsampling), then the gram loss is

$$\mathcal{L} = \|Z_S \cdot Z_S^\top - Z_T \cdot Z_T^\top\|_2^2$$

N is the number of patch representations and d is the size of each representation.

Using the gram matrices rather than the patch representations directly gives tolerance for sensor-specific differences in the high- and mid-resolution image pairs while penalising differences in patch-level spatial structure. Different from DINOv3’s “gram teacher” [11] whose parameters are selected from an earlier training iteration, our high-resolution encoder is updated along with the student encoder, as our goal in using the gram loss is to tolerate sensor-specific differences rather than maintain patch-level consistency across training progression.

B. Implementation and Evaluation

We pretrain both SSL schemes on the Sen2Venus dataset [10], which contains Sentinel 2 10-metre spatial resolution and Venus 5-meter spatial resolution image pairs collected on the same day. We sample a random 119,659 image pairs

and use only the red, green, blue and near-infrared bands. We train I-JEPA with a learning rate of 0.001 (cosine schedule), batch size of 64 and weight decay of 0.04 with AdamW, and LatentMIM with a learning rate of 0.00015, a batch size of 128, and weight decay of 0.05 with AdamW. Both I-JEPA and LatentMIM are pretrained for 300 epochs.

For I-JEPA [25], we use the ViT-Small architecture with a patch size of 14 for the target encoder, context encoders and high-resolution teacher, and a depth of 12 and embedding size of 384 for the predictor. For LatentMIM, we use the ViT-Small architecture with a patch size of 16 for the online encoder, target encoder and high-resolution teacher. We maintain LatentMIM’s decoder depth of 3.

We evaluate via linear probing on three Geo-Bench [28] benchmark datasets: m-cashew, m-sa-crop-type and MADOS. We use only the red, green, blue and near-infrared bands. We report results in mean Intersection over Union (mIoU) averaged over three runs.

IV. RESULTS

To demonstrate the superior semantic segmentation performance of using the spatial affinity component with a real mid- and high-resolution dataset, we compare three models pretrained on the same dataset with both I-JEPA and LatentMIM algorithms:

- 1) *MR-model*, pretrained on mid-resolution Sentinel-2 images only,
- 2) *HR-model*, pretrained on high-resolution Venus images only, and
- 3) *SA-model*, pretrained with the Spatial Affinity component on both mid- and high-resolution images.

The *MR-model* and *HR-model* are pretrained with the same input image size. Further, the mid-resolution input size of the *SA-model* matches the input size of the *MR*- and *HR* models.

Table I shows the downstream semantic segmentation performance of the three models pretrained with I-JEPA and LatentMIM. We see that the *SA-model* out-ranks the other models, demonstrating the superiority of adding a spatial affinity component to SSL pretraining and using real mid- and high-resolution image pairs.

TABLE I
LINEAR PROBING SEMANTIC SEGMENTATION PERFORMANCE
COMPARISON ACROSS FRAMEWORKS

Model	mIoU		
	m-Cashew	m-SA	MADOS
<i>I-JEPA Framework</i>			
MR-model	22.60	18.82	37.55
HR-model	24.25	19.46	40.94
SA-model	23.57	21.14	41.73
<i>LatentMIM Framework</i>			
MR-model	23.96	20.80	44.53
HR-model	24.89	21.95	44.84
SA-model	24.53	23.01	45.77

A. Super-Resolution

We investigate whether the downstream improvements come from the informational content of real high-resolution data or are merely a result of the addition of the spatial affinity objective. To test this, we compare the *SA-model* against a control model trained with ‘false’ high-resolution images generated via interpolation of the mid-resolution images. As shown in Table II, the model that uses real HR data outperforms the upsampled baseline in all cases, confirming the value of the high-resolution data in learning better representations of low-resolution data.

TABLE II
IMPACT OF REAL VS. FALSE HIGH-RESOLUTION IMAGERY ON
DOWNSTREAM SEMANTIC SEGMENTATION PERFORMANCE

Model	mIoU		
	m-Cashew	m-SA	MADOS
<i>I-JEPA Framework</i>			
w/ real HR	23.57	21.14	41.73
w/ false HR	22.26	19.70	36.41
<i>LatentMIM Framework</i>			
w/ real HR	24.53	23.01	45.77
w/ false HR	24.40	22.95	43.60

B. Qualitative View

We use the *MR*- and *HR*- and *SA*-models pretrained with I-JEPA to generate 64×64 patch representations of a Sentinel 2 image and cluster them using unsupervised hierarchical clustering into three classes to produce the cluster maps in Fig. 3.

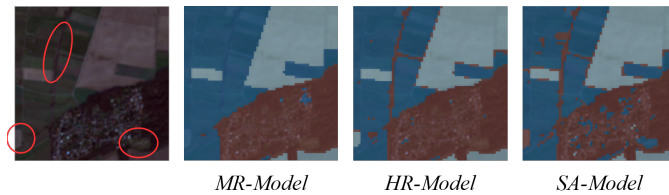


Fig. 3. Unsupervised cluster maps of the patch representations of a Sentinel 2 image with $k = 3$. Zoom in to see which model’s representations are able to identify the distinct features circled in red.

V. ABLATIONS

A. High-resolution Representation Downsampling

Due to the size difference stated in equation 1 between the mid- and high-resolution images, each patch in the mid-resolution image corresponds to s^2 patches in the high-resolution counterpart. Therefore, before applying the gram loss, we downsample the high-resolution patch representations to match the size of the mid-resolution patch representations. We downsample the s^2 high-resolution patches representations corresponding to a mid-resolution image patch to one patch representation. We test three downsampling methods: bilinear

and bicubic interpolation, and linear projection. Table III shows that bilinear downsampling results in better representations.

TABLE III
COMPARISON OF DOWNSAMPLING METHODS IN SPATIAL AFFINITY
COMPONENT WITH I-JEPA

Model	mIoU		
	m-Cashew	m-SA	MADOS
Bilinear	23.57	21.14	41.73
Bicubic	22.06	20.62	40.31
Linear projection	24.17	20.07	39.43

B. Sampling strategy

The spatial affinity component does not use all patches of its input image but rather samples a portion of the patches. Hypothesizing that contiguous patches carry spatial information better than random patches, we compare block sampling and LatentMIM’s default random sampling (see Fig. 2 (b) and (c) respectively). Table IV shows that using block sampling does not improve performance over using LatentMIM’s default random sampling.

TABLE IV
SPATIAL AFFINITY COMPONENT SAMPLING STRATEGY ABLATIONS ON
LATENTMIM

Model	mIoU		
	m-Cashew	m-SA	MADOS
Random	24.53	23.01	45.77
Block	21.80	20.65	44.53

VI. DISCUSSIONS

Our experiments show that integrating high-resolution satellite imagery data into mid-resolution pretraining using the spatial affinity component improves downstream semantic segmentation performance across diverse mid-resolution tasks over models pretrained with high- or mid-resolution imagery alone. This shows that effective methods of training with both HR and MR image data can exploit the advantages of either data to outperform models trained on only one of them. Given the scarcity of HR satellite imagery and thus the difficulty of acquiring good HR/MR image pair datasets, a promising direction for future work is to find methods to reduce reliance on good-quality image pairs.

REFERENCES

- [1] Y. Wang, N. A. A. Braham, Z. Xiong, C. Liu, C. M. Albrecht, and X. X. Zhu, “Ssl4eo-s12: A large-scale multimodal, multi-temporal dataset for self-supervised learning in earth observation [software and data sets],” *IEEE Geoscience and Remote Sensing Magazine*, vol. 11, no. 3, pp. 98–106, 2023.
- [2] Y. Cong, S. Khanna, C. Meng, P. Liu, E. Rozi, Y. He, M. Burke, D. Lobell, and S. Ermon, “Satmae: Pre-training transformers for temporal and multi-spectral satellite imagery,” *Advances in Neural Information Processing Systems*, vol. 35, pp. 197–211, 2022.

[3] J. Shermeyer and A. Van Etten, "The Effects of Super-Resolution on Object Detection Performance in Satellite Imagery/imagery," *IEEE Computer Society Conference on Computer Vision and Pattern Recognition Workshops*, vol. 2019-June, pp. 1432–1441, 6 2019. [Online]. Available: <https://ieeexplore.ieee.org/abstract/document/9025375>

[4] C. J. Reed, R. Gupta, S. Li, S. Brockman, C. Funk, B. Clipp, K. Keutzer, S. Candido, M. Uyttendaele, and T. Darrell, "Scale-mae: A scale-aware masked autoencoder for multiscale geospatial representation learning," in *Proceedings of the IEEE/CVF International Conference on Computer Vision*, 2023, pp. 4088–4099.

[5] V. Nedungadi, A. Kariryaa, S. Oehmcke, S. Belongie, C. Igel, and N. Lang, "Mmearth: Exploring multi-modal pretext tasks for geospatial representation learning," in *European Conference on Computer Vision*. Springer, 2024, pp. 164–182.

[6] D. Szwarcman, S. Roy, P. Fraccaro, O. E. Gíslason, B. Blumenstiel, R. Ghosal, P. H. De Oliveira, J. L. de Sousa Almeida, R. Sedona, Y. Kang *et al.*, "Prithvi-eo-2.0: A versatile multi-temporal foundation model for earth observation applications," *IEEE Transactions on Geoscience and Remote Sensing*, 2025.

[7] G. Tseng, A. Fuller, M. Reil, H. Herzog, P. Beukema, F. Bastani, J. R. Green, E. Shelhamer, H. Kerner, and D. Rolnick, "Galileo: Learning global & local features of many remote sensing modalities," *arXiv preprint arXiv:2502.09356*, 2025.

[8] C. F. Brown, M. R. Kazmierski, V. J. Pasquarella, W. J. Rucklidge, M. Samsikova, C. Zhang, E. Shelhamer, E. Lahera, O. Wiles, S. Ilyushchenko *et al.*, "Alphaearth foundations: An embedding field model for accurate and efficient global mapping from sparse label data," *arXiv preprint arXiv:2507.22291*, 2025.

[9] J. Jakubik, F. Yang, B. Blumenstiel, E. Scheurer, R. Sedona, S. Maurogiovanni, J. Bosmans, N. Dionelis, V. Marsocci, N. Kopp *et al.*, "Terramind: Large-scale generative multimodality for earth observation," *arXiv preprint arXiv:2504.11171*, 2025.

[10] J. Michel, J. Vinasco-Salinas, J. Inglada, and O. Hagolle, "Sen2venus, a dataset for the training of sentinel-2 super-resolution algorithms," *Data*, vol. 7, no. 7, 2022. [Online]. Available: <https://www.mdpi.com/2306-5729/7/7/96>

[11] O. Siméoni, H. V. Vo, M. Seitzer, F. Baldassarre, M. Oquab, C. Jose, V. Khalidov, M. Szafraniec, S. Yi, M. Ramamonjisoa *et al.*, "Dinov3," *arXiv preprint arXiv:2508.10104*, 2025.

[12] S. Hou, H. Shi, X. Cao, X. Zhang, and L. Jiao, "Hyperspectral Imagery Classification Based on Contrastive Learning," *IEEE Transactions on Geoscience and Remote Sensing*, vol. 60, 2022. [Online]. Available: <https://ieeexplore.ieee.org/document/9664575>

[13] K. Ayush, B. Uzkent, C. Meng, K. Tanmay, M. Burke, D. Lobell, and S. Ermon, "Geography-Aware Self-Supervised Learning," *Proceedings of the IEEE International Conference on Computer Vision*, pp. 10 161–10 170, 2021. [Online]. Available: <https://ieeexplore.ieee.org/abstract/document/9711401>

[14] N. Jean, S. Wang, A. Samar, G. Azzari, D. Lobell, and S. Ermon, "Tile2Vec: Unsupervised Representation Learning for Spatially Distributed Data," *Proceedings of the AAAI Conference on Artificial Intelligence*, vol. 33, no. 01, pp. 3967–3974, 7 2019. [Online]. Available: <https://ojs.aaai.org/index.php/AAAI/article/view/4288>

[15] Y. Wang, C. M. Albrecht, and X. X. Zhu, "Multilabel-Guided Soft Contrastive Learning for Efficient Earth Observation Pretraining," *IEEE Transactions on Geoscience and Remote Sensing*, vol. 62, 2024. [Online]. Available: <https://ieeexplore.ieee.org/abstract/document/10726860>

[16] Y. Gao, X. Sun, and C. Liu, "A General Self-Supervised Framework for Remote Sensing Image Classification," *Remote Sensing* 2022, Vol. 14, Page 4824, vol. 14, no. 19, p. 4824, 9 2022. [Online]. Available: <https://www.mdpi.com/2072-4292/14/19/4824>

[17] M. Tang, A. Cozma, K. Georgiou, H. Qi, and M. H. Kao, "Cross-Scale MAE: A Tale of Multiscale Exploitation in Remote Sensing," *Advances in Neural Information Processing Systems*, vol. 36, pp. 20 054–20 066, 12 2023.

[18] K. He, X. Chen, S. Xie, Y. Li, P. Dollár, and R. Girshick, "Masked autoencoders are scalable vision learners," in *Proceedings of the IEEE/CVF conference on computer vision and pattern recognition*, 2022, pp. 16 000–16 009.

[19] Y. Wei, A. Gupta, and P. Morgado, "Towards latent masked image modeling for self-supervised visual representation learning," in *European Conference on Computer Vision*. Springer, 2024, pp. 1–17.

[20] G. Christie, N. Fendley, J. Wilson, and R. Mukherjee, "Functional Map of the World," *Proceedings of the IEEE Computer Society Conference on Computer Vision and Pattern Recognition*, pp. 6172–6180, 12 2018. [Online]. Available: <https://ieeexplore.ieee.org/abstract/document/8578744>

[21] C. Chen, Z. Xiong, X. Tian, Z. J. Zha, and F. Wu, "Camera lens super-resolution," *Proceedings of the IEEE Computer Society Conference on Computer Vision and Pattern Recognition*, vol. 2019-June, pp. 1652–1660, 6 2019. [Online]. Available: <https://ieeexplore.ieee.org/abstract/document/8954317>

[22] J. Cai, H. Zeng, H. Yong, Z. Cao, and L. Zhang, "Toward real-world single image super-resolution: A new benchmark and a new model," *Proceedings of the IEEE International Conference on Computer Vision*, pp. 3086–3095, 10 2019. [Online]. Available: <https://ieeexplore.ieee.org/abstract/document/9009805>

[23] J. Li, X. Liang, Y. Wei, T. Xu, J. Feng, and S. Yan, "Perceptual generative adversarial networks for small object detection," *Proceedings - 30th IEEE Conference on Computer Vision and Pattern Recognition, CVPR 2017*, vol. 2017-January, pp. 1951–1959, 11 2017. [Online]. Available: <https://ieeexplore.ieee.org/abstract/document/8099694>

[24] J. Li, Z. Zhang, Y. Tian, Y. Xu, Y. Wen, and S. Wang, "Target-Guided Feature Super-Resolution for Vehicle Detection in Remote Sensing Images," *IEEE Geoscience and Remote Sensing Letters*, vol. 19, 2021. [Online]. Available: <https://ieeexplore.ieee.org/document/9548683>

[25] M. Assran, Q. Duval, I. Misra, P. Bojanowski, P. Vincent, M. Rabbat, Y. LeCun, and N. Ballas, "Self-supervised learning from images with a joint-embedding predictive architecture," in *Proceedings of the IEEE/CVF Conference on Computer Vision and Pattern Recognition*, 2023, pp. 15 619–15 629.

[26] M. Caron, H. Touvron, I. Misra, H. J'egou, J. Mairal, P. Bojanowski, and A. Joulin, "Emerging properties in self-supervised vision transformers," *2021 IEEE/CVF International Conference on Computer Vision (ICCV)*, pp. 9630–9640, 2021. [Online]. Available: <https://api.semanticscholar.org/CorpusID:233444273>

[27] A. Dosovitskiy, A. Kolesnikov, D. Weissenborn, G. Heigold, J. Uszkoreit, L. Beyer, M. Minderer, M. Dehghani, N. Houlsby, S. Gelly, T. Unterthiner, and X. Zhai, "An image is worth 16x16 words: Transformers for image recognition at scale," *arXiv preprint arXiv:2010.11929*, 2020.

[28] A. Lacoste, N. Lehmann, P. Rodriguez, E. D. Sherwin, H. Kerner, B. Lütjens, J. Irvin, D. Dao, H. Alemohammad, A. Drouin, M. Gunturkun, G. Huang, D. Vazquez, D. Newman, Y. Bengio, S. Ermon, and X. X. Zhu, "GEO-Bench: Toward Foundation Models for Earth Monitoring," *Advances in Neural Information Processing Systems*, vol. 36, pp. 51 080–51 093, 12 2023. [Online]. Available: <https://zenodo.org/communities/geo-bench>